Inorganic Chemistry

ARTICLE

pubs.acs.org/IC

Benzoannelation Stabilizes the d_{xy}^1 State of Low-Spin Iron(III) Porphyrinates

Takahisa Ikeue,*[,†] Makoto Handa,[†] Adam Chamberlin,[‡] Abhik Ghosh,*[,‡] Owendi Ongayi,[§] M. Graça H. Vicente,*[,§] Akira Ikezaki,[⊥] and Mikio Nakamura*[,⊥,¶]

[†]Department of Chemistry, Faculty of Material Science, Shimane University, 1060 Nishikawatsu-cho, Matsue-shi, Shimane 690-8504, Japan

[‡]Department of Chemistry and the Center for Theoretical and Computational Chemistry, University of Tromso, Breivika, N-9037 Tromso, Norway

[§]Department of Chemistry, Louisiana State University, Baton Rouge, Louisiana 70803, United States

[⊥]Department of Chemistry, School of Medicine, Toho University, Ota-ku, Tokyo 143-8540, Japan

[¶]Division of Chemistry, Graduate School of Science, Toho University, Funabashi 274-8510, Japan

Supporting Information

ABSTRACT: A series of low-spin, six-coordinate complexes [Fe(TBzTArP)L_2]X (**1**) and [Fe(TBuTArP)L_2]X (**2**) (X = Cl^-, BF_4^-, or Bu_4N^+), where the axial ligands (L) are HIm, 1-MeIm, DMAP, 4-MeOPy, 4-MePy, Py, and CN^-, were prepared. The electronic structures of these complexes were examined by ^{1}H NMR and electron paramagnetic resonance (EPR) spectroscopy as well as density functional theory (DFT) calculations. In spite of the fact that almost all of the bis(HIm), bis(1-MeIm), and bis(DMAP) complexes reported previously (including **2**) adopt the $(d_{xy})^2(d_{xz}, d_{yz})^3$ ground state, the corresponding complexes of **1** show the $(d_{xz}, d_{yz})^4(d_{xy})^1$ ground state at ambient temperature. At lower temperature, the electronic ground state of the HIm, 1-MeIm, and DMAP complexes of **1** changes to the common $(d_{xy})^2(d_{xz}, d_{yz})^3$ ground state. All of the other complexes of **1** and **2** carrying 4-MeOPy, 4-MePy, Py, and CN^- maintain the $(d_{xz}, d_{yz})^4(d_{xy})^1$ ground state in the NMR temperature range, i.e., 298−173 K. The EPR spectra taken at 4.2 K are fully consistent with the NMR results because the HIm and 1-MeIm complexes of **1** and **2** adopt the $(d_{xy})^2(d_{xz}, d_{yz})^3$ ground state, as revealed by the rhombic-type spectra. The DMAP complex of **1** exists as a mixture of two electron-configurational isomers. All of the other complexes adopt the $(d_{xz}, d_{yz})^4(d_{xy})^1$ ground state, as revealed by the axial-type spectra. Among the complexes adopting the $(d_{xz}, d_{yz})^4(d_{xy})^1$ ground state, the energy gap between the d_{xy} and d_π orbitals in **1** is always larger than that of the corresponding complex of **2**. Thus, it is clear that the benzoannelation of the porphyrin ring stabilizes the $(d_{xz}, d_{yz})^4(d_{xy})^1$ ground state. The DFT calculation of the bis(Py) complex of analogous iron(III) porphyrinate, $[Fe(TPTBzP)(Py)_2]^+$, suggests that the $(d_{xz}, d_{yz})^4(d_{xy})^1$ state is more stable than the $(d_{xy})^2(d_{xz}, d_{yz})^3$ state in both ruffled and saddled conformations. The lowest-energy states in the two conformers are so close in energy that their ordering is reversed depending on the calculation methods applied. On the basis of the spectroscopic and theoretical results, we concluded that **1**, having 4-MeOPy, 4-MePy, and Py as axial ligands, exists as an equilibrium mixture of saddled and ruffled isomers both of which adopt the $(d_{xz}, d_{yz})^4(d_{xy})^1$ ground state. The stability of the $(d_{xz}, d_{yz})^4(d_{xy})^1$ ground state is ascribed to the strong bonding interaction between the iron d_{xy} and porphyrin a_{1u} orbitals in the saddled conformer caused by the high energy of the a_{1u} highest occupied molecular orbital in TBzTArP. Similarly, a bonding interaction occurs between the d_{xy} and a_{2u} orbitals in the ruffled conformer. In addition, the bonding interaction of the d_π orbitals with the low-lying lowest unoccupied molecular orbital, which is an inherent characteristic of TBzTArP, can also contribute to stabilization of the $(d_{xz}, d_{yz})^4(d_{xy})^1$ ground state.

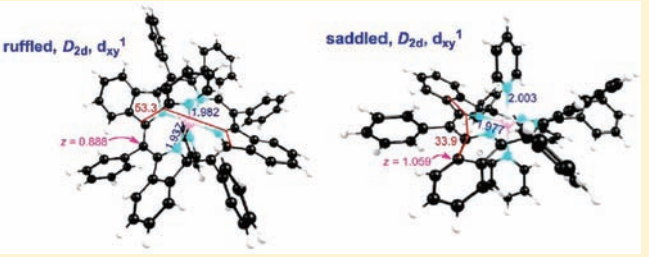

INTRODUCTION

Six-coordinate, low-spin iron(III) porphyrinates adopt either the common $(d_{xy})^2(d_{xz}, d_{yz})^3$ or the less common $(d_{xz}, d_{yz})^4(d_{xy})^1$ ground state, as shown in Scheme 1, depending on various factors including the nature and number of axial ligands, electronic effects of peripheral substituents, deformation of the porphyrin ring, etc.[1−8] Among these factors, the nature and number of the axial ligands must be of primary importance. For example, axial ligands with strong σ-donating and weak π-accepting ability such as imidazole (HIm) and 4-(*N*,*N*-dimethylamino)pyridine (DMAP) stabilize the $(d_{xy})^2(d_{xz}, d_{yz})^3$ ground state. In contrast,

Received: December 13, 2010
Published: March 16, 2011

axial ligands with strong π-accepting ability such as *tert*-butylisocyanide (^{t}BuNC) and 4-CNPy stabilize the d_π orbital by $d_\pi-p_{\pi^*}$ interactions and lead to the formation of complexes with the less common $(d_{xz}, d_{yz})^4(d_{xy})^1$ ground state.[9−13] The latter ground state is further stabilized[14−22] by the ruffled deformation of the porphyrin ring.[14−27] This is because the iron d_{xy} orbital is destabilized relative to the d_π orbitals because of an interaction between the porphyrin a_{2u} and iron d_{xy} orbitals, which is symmetry-allowed in a ruffled D_{2d} framework.[28,29] As an extension of our long-term studies of unusual electronic structure of ion porphyrins and porphyrinoids, we examined the ^{1}H NMR and electron paramagnetic resonance (EPR) spectra of low-spin, six-coordinate $[Fe(TBzTArP)L_2]X$ (**1**) and compared the spectroscopic data with those of the corresponding $[Fe(TBuTArP)L_2]X$ (**2**) and $[Fe(OETPP)L_2]X$ (**3**; where $OETPP^{2-}$ = dianion of 2,3,7,8,12,13,17,18-octaethyl-5,10,15,20-tetraphenylporphyrin) to reveal the effect of benzoannelation on the electronic structure of low-spin iron(III) complexes, where the axial ligands (L) examined are HIm (**a**), 1-methylimidazole (1-MeIm; **b**), DMAP (**c**), 4-methoxypyridine (4-MeOPy; **d**), 4-methylpyridine (4-MePy; **e**), pyridine (Py; **f**), 4-CNPy (**g**), and CN^- (**h**) and the counteranion or cation (X) is Cl^-, BF_4^-, or Bu_4N^+ (Scheme 2).

RESULTS

^{1}H NMR Spectra. Figure 1 shows the ^{1}H NMR spectra of series $[Fe(TBzTArP)L_2]^{\pm}$ [**1**; L = HIm, DMAP, 4-MeOPy, and CN^-, where $TBzTArP^{2-}$ = dianion of 2:3,7:8,12:13,17:18-tetrabenzo-5,10,15,20-tetrakis(4-nonylphenyl)porphyrin] taken in CD_2Cl_2 solutions at 233 K. The ^{1}H NMR spectra of other complexes are given in Figure S1 of the Supporting Information (SI).

Scheme 1. Two Types of Electronic Ground States

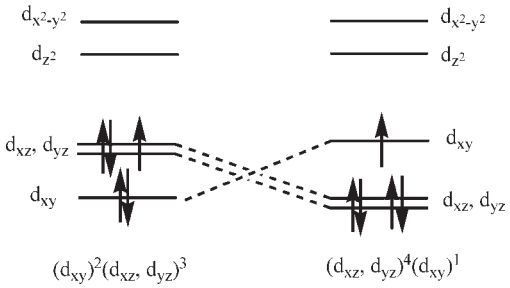

Similarly, the ^{1}H NMR spectra of series $[Fe(TBuTArP)L_2]^{\pm}$ (**2**; where $TBuTArPP^{2-}$ = dianion of 2:3,7:8,12:13,17:18-tetrabutano-5,10,15,20-tetrakis(4-nonylphenyl)porphyrin] are given in

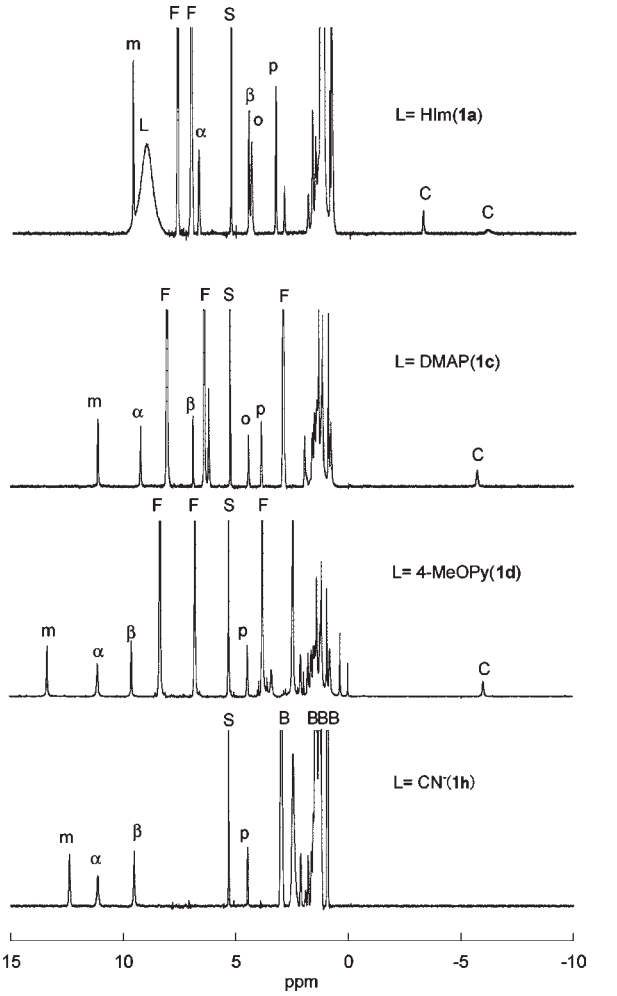

Figure 1. ^{1}H NMR spectra of **1a**, **1c**, **1d**, and **1h** taken in a CD_2Cl_2 solution at 233 K. Resonances signified as o, m, p, α, *β*, C, F, and S indicate the *o*-H, *m*-H, *p*-$CH_2(\alpha)$, α-H, *β*-H, coordinated ligand H, free ligand H, and solvent signals, respectively. B indicates the butyl H of tetrabutylammonium cyanide.

Scheme 2. Complexes 1 and 2 Examined in This Study Together with the Labels for Some Carbon Positions[a]

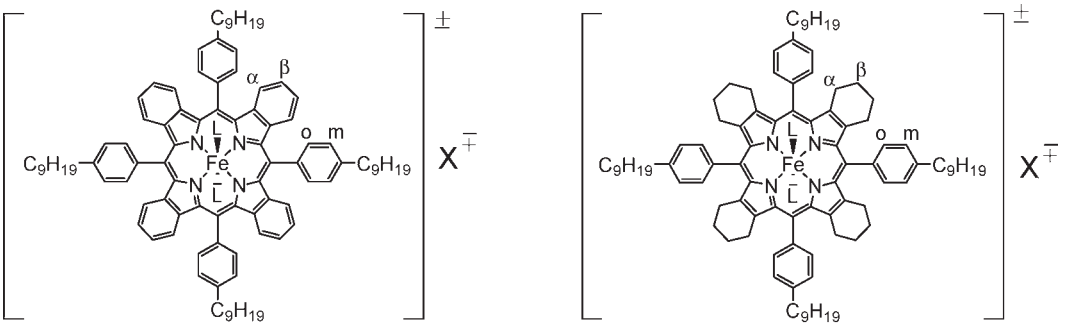

[a] Axial ligands (L) are as follows: **a**, HIm; **b**, 1-MeIm; **c**, DMAP; **d**, 4-MeOPy; **e**, 4-MePy; **f**, Py; **g**, 4-CNPy; **h**, CN^-. The countercation or -anion (X) is Cl^-, BF_4^-, or Bu_4N^+.

dx.doi.org/10.1021/ic1024873 |*Inorg. Chem.* 2011, 50, 3567–3581

Table 1. ^{1}H NMR Chemical Shifts Determined in a CD_2Cl_2 Solution at 298 K (Upper) and 213 K (Lower)

		chemical shifts (δ, ppm)									
L	T (K)	α	β	ortho	meta	p-CH_2	ligand[a]			$\delta_m - \delta_o$	slope[b]
						$[Fe(TBzTArP)L_2]^{\pm}$ (**1**)					
HIm (**a**)	298	7.77	5.85	5.27	9.85	3.54				4.62	+ → −
	213	6.32	3.89	4.37	9.47	3.23	−21.31	−5.10	−2.82	5.10	
1-MeIm (**b**)	298	8.15	6.31	5.18	10.32	3.70				5.14	+ → −
	213	8.13	5.74	4.33	10.86	3.73	−21.85	−6.02	−10.46 (3.73)	6.53	
DMAP (**c**)	298	8.79	6.94	4.99	10.48	3.73				5.49	+ → −
	213	9.28	6.76	4.26	11.31	3.90	−29.91		−6.41 (6.87)	7.05	
4-MeOPy (**d**)	298	9.92	8.68	4.24	11.78	4.23				7.54	+
	213	11.63	9.97	3.18	13.94	4.61	−28.10		−7.11 (0.03)	10.76	
4-MePy (**e**)	298	9.78	8.78	3.91	12.20	4.17				8.29	+
	213	11.53	10.17	2.77	14.24	4.66	−26.30		−7.80 (−3.91)	11.47	
Py (**f**)	298	9.76	8.93	3.66	12.48	4.22				8.82	+
	213	11.45	10.31	2.32	14.48	4.53	−24.20		−7.29	12.16	
CN^- (**h**)	298	10.05	8.60	5.35	11.16	4.04				5.84	+
	213	11.54	9.86	4.26	12.88	4.62				8.62	
						$[Fe(TBuTArP)L_2]^{\pm}$ (**2**)					
HIm (**a**)	298	29.67	0.65	5.77	6.60	2.35				0.83	−
	213	28.68	−0.63	3.88	5.78	1.78	−12.96		14.96	1.89	
1-MeIm (**b**)	298	29.84	0.75	5.77	6.74	2.35				0.97	−
	213	31.20	−0.38	3.99	5.81	1.83	−11.56		(17.31)	1.82	
DMAP (**c**)	298	24.19	0.55	5.28	6.73	2.39				1.45	−
	213	28.05	−0.32	3.77	6.35	1.99	−16.64		8.49(16.68)	2.58	
4-MeOPy (**d**)	298	29.12	0.90	6.25	7.76	2.85				1.51	+
	213	24.00	0.85	4.64	8.51	2.92	−27.42			3.87	
4-MePy (**e**)	298	28.59	1.71	6.34	8.29	3.01				1.95	+
	213	20.18	0.85	4.63	9.47	3.15	−31.06	−1.35		4.84	
Py (**f**)	298	28.94[c]	1.80[c]	5.61[c]	8.72[c]	3.15[c]				3.11	+
	213	16.49	2.76	4.34	10.53	3.54	−5.00	−1.30		6.19	
4-CNPy (**g**)	298	68.14[c]	2.10[c]	3.04[c]	7.66[c]	1.97[c]				4.62	curve[d]
	213	9.75	3.04	4.18	12.80	1.99	−31.06	−1.35		8.62	
CN^- (**h**)	298	9.56	2.04	6.14	9.15	3.33				3.01	+
	213	8.75	2.74	5.86	10.43	3.68				4.77	
						$[Fe(OETPP)L_2]^{\pm}$ (**3**)[e]					
HIm (**a**)[f,g]	298	7.34[h]	0.86	4.97	5.80	(6.73)				0.83	
	213	4.98[h]	1.34	2.44	4.50	(5.87)	21.66	16.53	14.21	2.06	
DMAP (**c**)[f,g]	298	8.26[h]	0.83	5.36	5.87	(6.88)				0.51	
	213	7.93[h]	1.42	2.36	4.65	(5.78)	16.51		−2.87(19.06)	2.29	
Py (**f**)[f]	298	21.68[h]	−0.39	13.01	5.77	(10.41)				−7.24	
	213	16.93[h]	0.58	6.96	5.03	(7.78)	32.80		21.15	−1.93	
4-CNPy (**g**)[f,i]	298	27.75[h]	−0.66	16.46	5.32	(12.11)				−11.14	
	213	39.15[h]	−0.70	19.88	3.98	(14.01)	76.16		58.43	−15.90	
CN^- (**h**)[j]	298	6.87	0.78	5.41	6.45	(6.58)				1.04	
	213	7.89	0.77	3.49	5.59	(5.86)				2.10	
^{t}BuNC[j,k]	298	7.46	1.09	5.54	11.05	(6.31)	(−1.52)			5.51	
	213	9.78	1.15	6.04	11.53	(6.51)	(−3.17)			5.49	
THF[i,j]	298	26.13	0.35	15.79	5.74	(11.48)				−10.05	
	213	32.21	1.15	19.06	4.68	(12.97)				−14.38	

[a] Data in parentheses are the chemical shifts of the methyl signals in the coordinating ligand. [b] Slope of the Curie plots of the m-H signals. + → − indicates that the slope changes from + to − as the temperature is lowered. [c] Extrapolated value. [d] See the text. [e] Data in parentheses are the chemical shifts of the p-H signal. [f] Reference 30. [g] The low-spin complex that adopts the $(d_{xy})^2(d_{xz}, d_{yz})^3$ ground state. [h] Averaged chemical shifts of the CH_2 (α) signals. [i] The complex that adopts the pure $S = {}^3/_2$ ground state. [j] Reference 22. [k] The low-spin complex that adopts the $(d_{xz}, d_{yz})^4(d_{xy})^1$ ground state.

dx.doi.org/10.1021/ic1024873 |*Inorg. Chem.* 2011, 50, 3567–3581

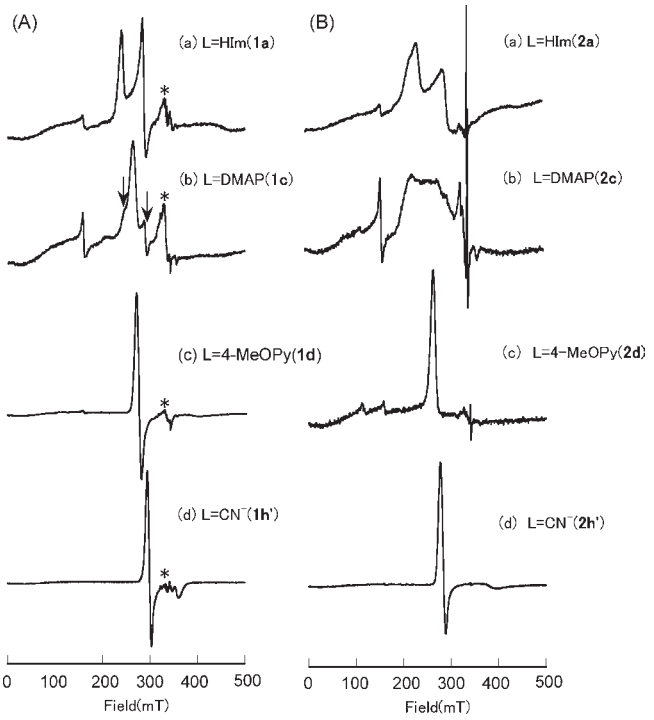

Figure 2. EPR spectra of (A) **1** and (B) **2** taken in frozen CH_2Cl_2 solutions at 4.2 K, where a−d correspond to the complexes carrying HIm, DMAP, 4-MeOPy, and CN^- (in MeOH). The impurity peaks are indicated by asterisks.

Figure S2a,b of the SI. The signal assignment will be described in the Discussion section. Table 1 lists the chemical shifts of **1** and **2** determined at 298 and 213 K.

EPR Spectra. EPR spectra of **1** and **2** were taken in frozen CH_2Cl_2 solutions at 4.2 K. Some of them are given in Figure 2. EPR spectra of other complexes are given in Figure S3a,b of the SI. As shown in Figure 2A, each spectrum of **1** contains some signals around g = 2.08 (indicated by asterisks), which are presumably ascribed to the decomposed species. The intensities of the impurity signals are much smaller in the case of **2**, as shown in Figure 2B, although some complexes exhibit a sharp signal at g = 2.01 caused by the organic free radical. In the case of **2c**, the signals are poorly resolved. The g values of the major signals of **1** and **2** are listed in Table 2 together with those of analogous **3**.[22,30] The tetragonal splitting (Δ/λ) values, which indicate the energy difference between the d_{xy} and d_π(d_{xz} and d_{yz}) orbitals, are also listed in Table 2 in units of the spin−orbit coupling constant (λ). A negative value of Δ/λ indicates that the d_{xy} orbital is located above the d_{xz} and d_{yz} orbitals.[31−33]

DFT Calculations. DFT calculations[28,29,34−38] were carried out to examine the relative stabilities of the $(d_{xz}, d_{yz})^4(d_{xy})^1$ and $(d_{xy})^2(d_{xz}, d_{yz})^3$ states of both the ruffled and saddled conformations in the bis(Py) complex of structurally similar iron(III) porphyrinate, i.e., $[Fe(TBzTPP)(Py)_2]^+$ (where TPP^{2-} = dianion of 5,10,15,20-tetraphenylporphyrin and $TBzTPP^{2-}$ = dianion of 2:3,7:8,12:13,17:18-tetrabenzo-5,10,15,20-tetraphenylporphyrin). Intermediate ruffled−saddled geometries were also examined; however, these relaxed to either the pure ruffled or the pure saddled geometry. In addition, we also optimized both the ruffled and saddled conformations of four-coordinate nickel(II), copper(II), and zinc(II) complexes of TBzTPP, all of which exhibited a clear preference for the saddled conformation. Table 3 presents the energetics of

Table 2. EPR g Values and Tetragonal Splitting (Δ/λ) Values[a]

ligand (L)	g values			Δ/λ[b]	ref
	$[Fe(TArTBzP)L_2]^{\pm}$ (**1**)				
HIm (**a**)	2.80	2.38	1.47		tw
1-MeIm (**b**)	2.85	2.40	1.44		tw
DMAP (**c**)[c]	2.53				tw
	2.77	2.36			
4-MeOPy (**d**)	2.49		1.71	−3.5	tw
4-MePy (**e**)	2.43		1.77	−4.1	tw
Py (**f**)	2.40		1.83	−4.5	tw
CN^- (**h**)	2.39		1.81	−4.5	tw
CN^- (**h′**) (CH_3OH)	2.29		1.90	−6.3	tw
	$[Fe(TArTBuP)L_2]^{\pm}$(**2**)				
HIm (**a**)	2.97	2.34	1.53		tw
1-MeIm (**b**)	3.03	2.34	1.56		tw
DMAP (**c**)[d]	3.0				tw
4-MeOPy (**d**)	2.58				
4-MePy (**e**)	2.53				tw
Py (**f**)	2.54				tw
4-CNPy (**g**)	2.47		1.70	−3.7	tw
CN^- (**h**)	2.50				tw
CN^- (**h′**) (CH_3OH)	2.39		1.73	−4.0	tw
	$[Fe(OETPP)L_2]^{\pm}$ (**3**)				
HIm (**a**)	2.72	2.37	1.64		22
DMAP (**c**)	3.06	2.14	1.42		30
Py (**f**)	3.39	2.08			30
4-CNPy (**g**)[e]	4.28	3.80	2.08		30
^{t}BuNC[f]	2.29	2.25	1.92		22
THF[e]	4.01		2.00		22

[a] Frozen CH_2Cl_2 solutions at 4.2 K. [b] Tetragonal parameters where λ is a spin−orbit coupling constant. Negative values indicate that the d_{xy} orbital is higher than the d_π orbital. [c] Two species coexist. See the text. [d] Signals are too broad. [e] The pure intermediate-spin ($S = {}^3/_2$) complex. [f] The low-spin complex that adopts the pure $(d_{xz}, d_{yz})^4(d_{xy})^1$ ground state.

different states $[Fe(TBzTPP)(Py)_2]^+$ for a number of different exchange-correlation functionals, including two with dispersion corrections. The four states examined for this complex are all rather close in energy, and indeed their relative ordering varies somewhat depending on the DFT method used; thus, on the basis of these calculations alone, it would be difficult to make an unequivocal prediction about the actual experimental structure and conformation. Spectroscopic data and the calculations together, however, do point toward a preferred state for this complex.

As shown in Table 3, regardless of whether one assumes a ruffled or a saddled conformation, the calculations favor a $(d_{xz}, d_{yz})^4(d_{xy})^1$ state over a $(d_{xy})^2(d_{xz}, d_{yz})^3$ state. However, deciding between a ruffled or a saddled conformation is more difficult. Thus, whereas OLYP,[39,40] BP86[41,42] and BLYP[41−44] all indicate a saddled $(d_{xz}, d_{yz})^4(d_{xy})^1$ state as the lowest-energy state, including Grimme's[45] dispersion correction results in a reversal of the lowest-energy states; thus, BP86-D indicates a ruffled $(d_{xz}, d_{yz})^4(d_{xy})^1$ state as the ground state, whereas BLYP-D predicts almost exactly equienergetic ruffled and saddled $(d_{xz}, d_{yz})^4(d_{xy})^1$ states. Considering how delicately the different conformational and spin states are balanced, one must be careful indeed with ascribing the stability of a state to a

dx.doi.org/10.1021/ic1024873 |Inorg. Chem. 2011, 50, 3567–3581

Table 3. Electronic Configurations, Conformations, and OLYP/TZP Energies of $S = {}^1/_2$ $[Fe(TBzTPP)(Py)_2]^+$

				energy (eV)				
state	iron config.	geometry	all-electron occupations ($\alpha//\beta$)	OLYP	BP86	BP86-D	BLYP	BLYP-D
A	$(d_{xz}, d_{yz})^4(d_{xy})^1$	ruffled (D_{2d})	a_1 50//50	0.00	0.00	0.00	0.00	0.00
			a_2 18//18					
			b_1 21//21					
			b_2 48//47					
			e 130//130					
B	$(d_{xz}, d_{yz})^3(d_{xy})^2$	ruffled (C_{2v})	a_1 98//98	0.23	0.24	0.26	0.22	0.24
			a_2 39//39					
			b_1 65//65					
			b_2 65//64					
C	$(d_{xz}, d_{yz})^4(d_{xy})^1$	saddled (D_{2d})	a_1 45//45	−0.30	−0.10	0.11	−0.23	0.01
			a_2 23//23					
			b_1 28//27					
			b_2 41//41					
			e 130//130					
D	$(d_{xz}, d_{yz})^3(d_{xy})^2$	saddled (C_{2v})	a_1 86//86	−0.14	0.05	0.26	−0.06	0.17
			a_2 51//51					
			b_1 65//65					
			b_2 65//64					

Table 4. OLYP/TZP Mulliken Spin Populations for Different States of $S = {}^1/_2$ $[Fe(TBzTPP)(Py)_2]^+$

atom	A	B	C	D
Fe	0.7402	0.9389	0.3307	0.9266
N_{Por}	0.0416	−0.0062	−0.0293	−0.0176, 0.0116
C_α	−0.0216	0.0128	0.0900	0.0034, 0.0060
C_β	−0.0001	0.0044	−0.0078	−0.0030, 0.0203
C_{meso}	0.0878	−0.0001, −0.0052	−0.0344	−0.0078
$C_{i\text{-}Ph}$	−0.0054	0.0005	0.0040	0.0008
$C_{o\text{-}Ph}$	0.0020	−0.0001	−0.0014	−0.0005
$C_{m\text{-}Ph}$	−0.0003	0.0002	0.0004	0.0001
$C_{p\text{-}Ph}$	0.0002	−0.0001	−0.0009	−0.0002
N_{Py}	−0.0098	−0.0252	−0.0059	−0.0219
$C_{\alpha\text{-}Py}$	−0.0043	−0.0024	−0.0019	−0.0012

specific metal−ligand orbital interaction, although we will *attempt* to do so.

As shown in Table 4, the ruffled and $(d_{xz}, d_{yz})^4(d_{xy})^1$ states exhibit significant positive spin populations on the *meso*-C atoms, attributable to the Fe(d_{xy})−porphyrin(a_{2u}) orbital interaction, which is shown in Figure 3. Interestingly, the saddled $(d_{xz}, d_{yz})^4(d_{xy})^1$ state also has significant meso spin populations; these, however, are negative spin populations. This state features an unusually strong Fe(d_{xy})−porphyrin-(a_{1u}) orbital interaction, resulting in an exceedingly small Fe spin population and large quantities of positive spin on the TBzTPP ligand; this is shown in Table 4 and in Figures 4 and 5. The strength of this orbital interaction is a result of the high energy of the TBzTPP a_{1u} highest occupied molecular orbital (HOMO);[46] thus, for closed-shell derivatives such as a free base or Zn^{II}TBzTPP, the a_{1u} HOMO is far higher in energy (i.e., corresponding to a lower ionization potential) than the a_{2u} HOMO, with the latter being similar in energy to that in an analogous TPP complex.

The optimized geometries of the different electronic states are relatively unremarkable. We will therefore limit ourselves to briefly describing the ruffled and saddled $(d_{xz}, d_{yz})^4(d_{xy})^1$ states (Figure 6), the two nearly equienergetic contenders for the ground state. Both states deviate quite strongly from planarity. Thus, adjacent pyrrole rings in the saddled conformation are tilted by just over 30° relative to each other, whereas antipodal pyrrole rings in the ruffled conformation are twisted by over 50° relative to each other. As expected, the Fe−N_{Por} distances are significantly shorter in the ruffled conformation (1.937 Å) than in the saddled conformation (1.977 Å). Overall, this is a remarkable and indeed unique example of a porphyrin derivative whose ruffled and saddled conformations are almost identical in energy.

DISCUSSION

Signal Assignments in ^{1}H NMR Spectra. The signals were assigned by the 2D COSY spectra, which are given in Figure S4a−d of the SI. In the case of **1e**, the signal at 2.1 ppm showed the correlation with the two signals at 1.8 and 4.5 ppm. Thus, the signals at 2.1, 1.8, and 4.5 ppm were assigned to *p*-$CH_2(\beta)$, *p*-$CH_2(\gamma)$, and *p*-$CH_2(\alpha)$, respectively. The downfield shift of the *p*-$CH_2(\alpha)$ signal is a direct indication that the *meso*-C atoms have a sizable amount of spin density, which should induce the upfield and downfield shifts to the *o*-H and *m*-H signals, respectively. Thus, the two signals at 13.7 and 3.1 ppm, which exhibited the correlation peak, were assigned to the *m*-H and *o*-H signals, respectively. Another correlation was observed between the two signals at 11.1 and 9.8 ppm. Thus, they belong to the fused benzene ring. The assignment of α-H and *β*-H is quite difficult. We tentatively assigned the broader and more downfield shifted signal to α-H because these complexes adopt the $(d_{xz}, d_{yz})^4(d_{xy})^1$ ground state as mentioned in the following section; the low-spin complexes with the $(d_{xz}, d_{yz})^4(d_{xy})^1$ ground state induces a positive dipolar shift to the protons on the porphyrin ring.

Methodology To Determine the Electronic Ground State. *1. NMR Method.* Electronic ground states can be determined

dx.doi.org/10.1021/ic1024873 |*Inorg. Chem.* 2011, 50, 3567–3581

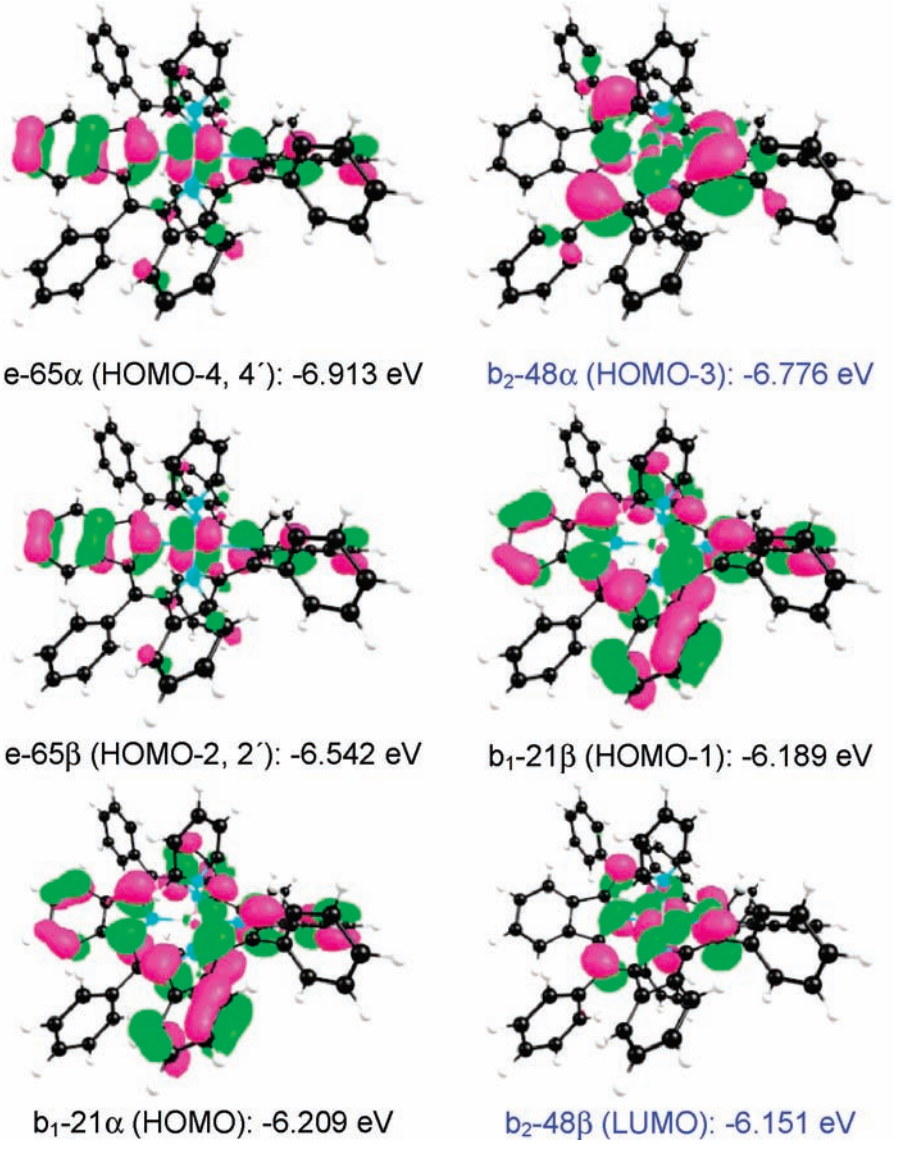

Figure 3. Selected frontier MOs of the ruffled $(d_{xz}, d_{yz})^4(d_{xy})^1$ state of $[Fe(TBzTPP)]^+$ (i.e., state C). The spin-unrestricted MOs that best correspond to a singly occupied MO are indicated by a blue legend.

by the ^{1}H and ^{13}C NMR spectra.[2−8] In the complexes with the $(d_{xy})^2(d_{xz}, d_{yz})^3$ ground state, the unpaired electron in the d_π orbitals can be delocalized to the porphyrin ring especially on the pyrrole β-C atoms and induces the upfield shift of the pyrrole β-H signals. In the complexes with the $(d_{xz}, d_{yz})^4(d_{xy})^1$ ground state, the unpaired electron in the d_{xy} orbital can be delocalized to the ruffled porphyrin ring especially on the *meso*-C atoms by interaction with the porphyrin a_{2u} orbital;[2−8] the a_{2u} orbital has a large coefficient at the *meso*-C atoms. Thus, we can expect that the *o*-H and *p*-H signals appear upfield, while the *m*-H signal appears downfield in the complexes having phenyl groups at the meso positions.

Our previous papers showed that even the highly saddled $[Fe(OETPP)(^tBuNC)_2]^+$ with the $(d_{xz}, d_{yz})^4(d_{xy})^1$ ground state exhibits the *meso*-C and *m*-H signals fairly downfield, 416 and 11.1 ppm, respectively, at 298 K.[22] The reason for the downfield shift of the *meso*-C and *m*-H signals in highly saddled $(d_{xz}, d_{yz})^4(d_{xy})^1$-type complexes is not clear at this point. Presumably, the saddled porphyrin ring in the solid state is ruffled to some extent in solution, which will be discussed later.

We chose the *m*-H signal as a probe to reveal the electronic structure of series **1**. The theoretical background is given below.[47−50] The observed chemical shift (δ_{obs}) of the *m*-H signal can be given by eq 1, where δ_{iso} is the isotropic shift and δ_{dia} is the chemical shift of the *m*-H signal in a suitable diamagnetic complex. The δ_{iso} value, which is the sum of the contact shift (δ_{con}) and dipolar shift (δ_{dip}), can be expressed as eq 2 in the case of complexes with axial symmetry, where K_{con} and K_{dip} are positive constants, ρ_C is a spin density at the *m*-C atom, and $(3\cos^2\theta - 1)/r^3$ is a geometric factor of the *m*-H atom.

$$\delta_{obs} = \delta_{iso} + \delta_{dia} \quad (1)$$

$$\delta_{iso} = \delta_{con} + \delta_{dip} = [-K_{con}\rho_C + K_{dip}(g_{||}^2 - g_{\perp}^2)(3\cos^2\theta - 1)/r^3]/T \quad (2)$$

In the low-spin complexes with the $(d_{xy})^2(d_{xz}, d_{yz})^3$ ground state, the spin density at the *meso*-C atom is supposed to be zero because the major interaction takes place between the half-filled

dx.doi.org/10.1021/ic1024873 |*Inorg. Chem.* 2011, 50, 3567–3581

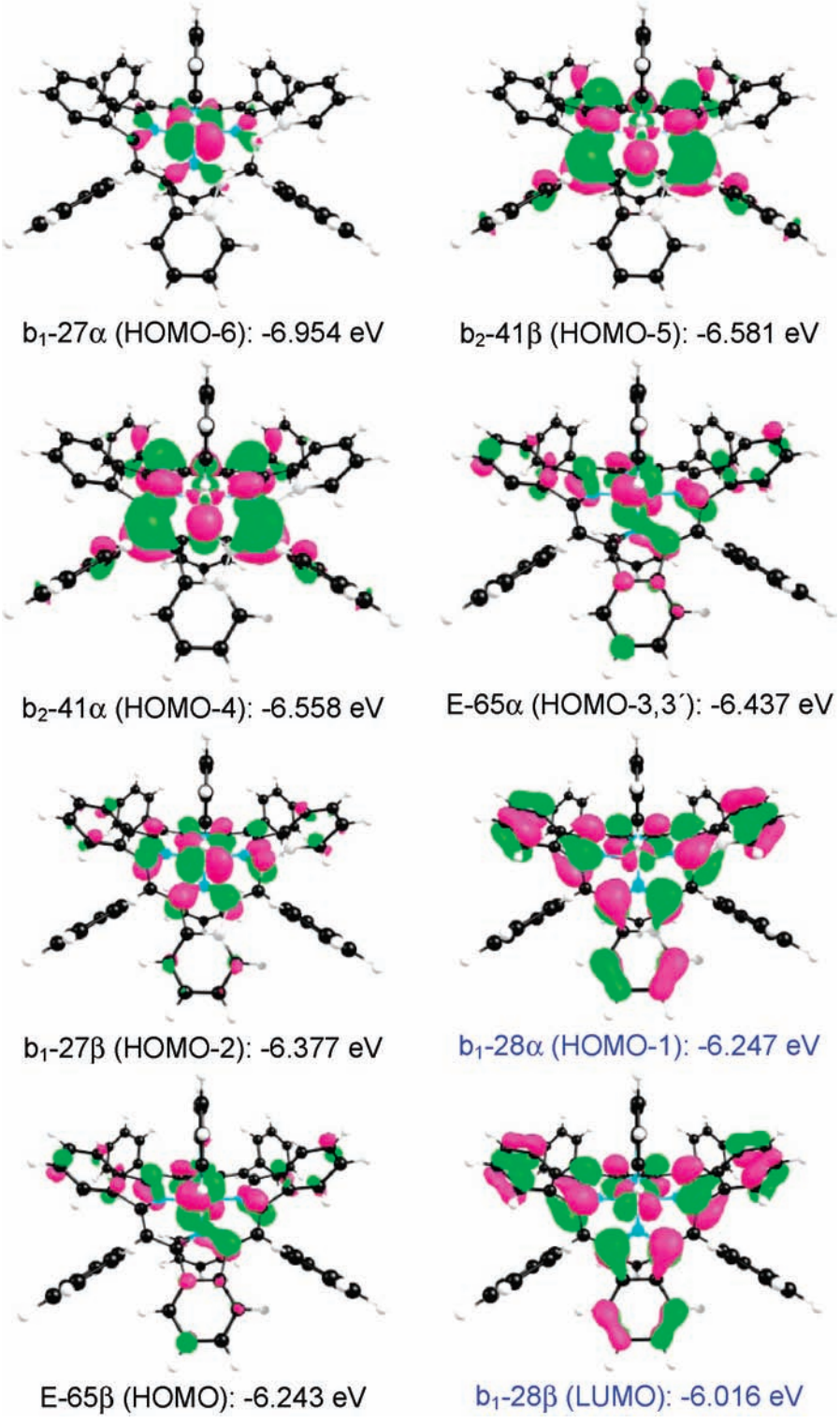

Figure 4. Selected frontier MOs of the saddled $(d_{xz}, d_{yz})^4(d_{xy})^1$ state of $[Fe(TBzTPP)]^+$ (i.e., state A). The spin-unrestricted MOs that best correspond to a singly occupied MO are indicated by a blue legend.

d_π and filled porphyrin $3e_g$ orbitals; the $3e_g$ orbitals have a negligibly small coefficient at the *meso*-C atoms. Thus, the slope of the Curie plots for the *m*-H signal should be negative because ρ_C at the *m*-C atom is nearly zero and $(g_\parallel{}^2 - g_\perp{}^2)(3\cos^2\theta - 1)/r^3$ is negative; note that $g_\parallel{}^2 - g_\perp{}^2$ is positive, while $(3\cos^2\theta - 1)/r^3$ is negative for *m*-H.

In the $(d_{xz}, d_{yz})^4(d_{xy})^1$-type ruffled complexes, the *meso*-C atom has a sizable amount of spin density because of interaction between the half-occupied d_{xy} and filled a_{2u} orbitals. The positive spin at the *meso*-C atoms is delocalized to the attached phenyl groups and induces the negative π spin density at the *m*-C atoms. Thus, the slope for the contact shift, $-K_{con}\rho_C$, should be positive.

dx.doi.org/10.1021/ic1024873 |*Inorg. Chem.* 2011, 50, 3567–3581

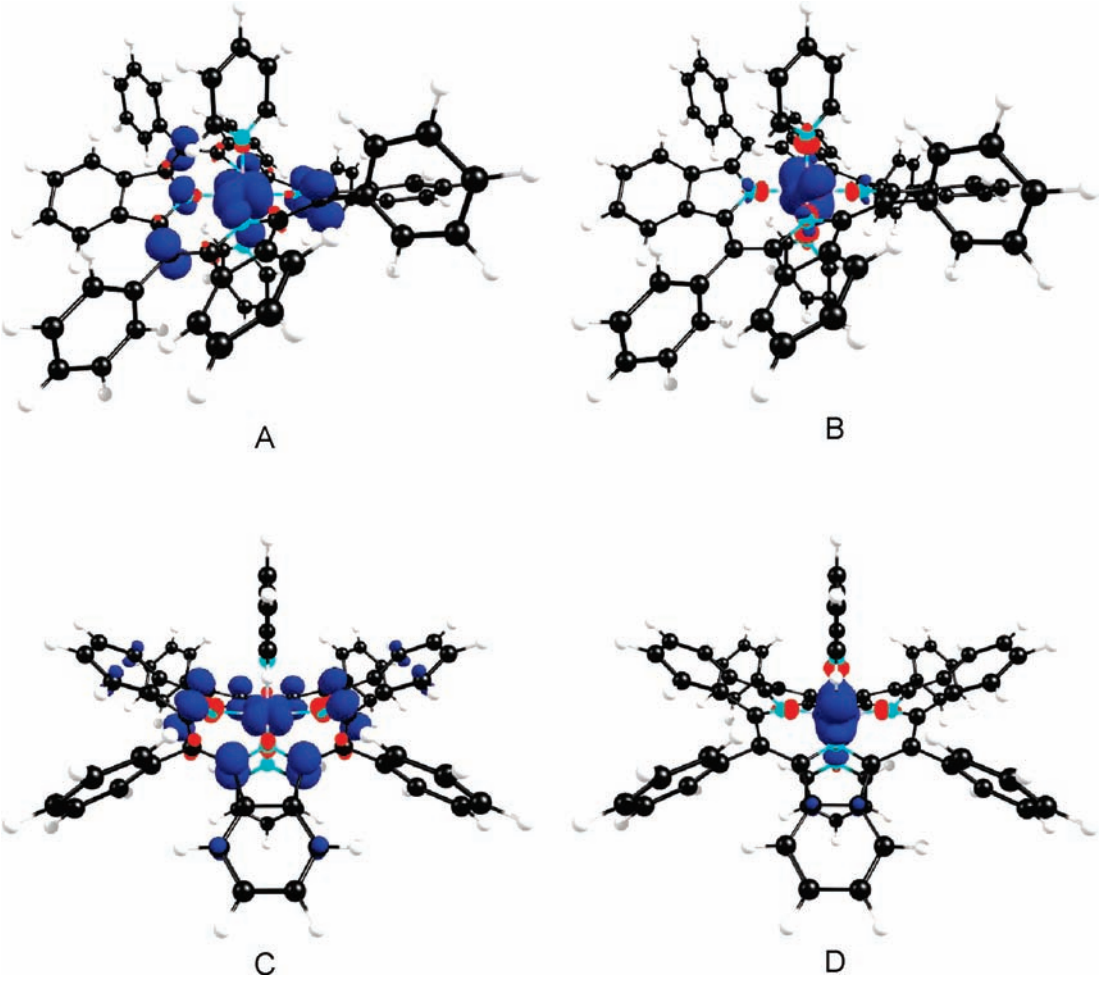

Figure 5. Spin densities (0.0025 e/Å^3) for states A−D for $[Fe(TBzTPP)]^+$. Majority and minority spin densities are indicated in blue and red, respectively.

In addition, the slope for the dipolar shift, $(g_{\parallel}{}^2 - g_{\perp}{}^2)(3\cos^2\theta - 1)/r^3$, should also be positive because the $g_{\parallel}{}^2 - g_{\perp}{}^2$ value is negative in the $(d_{xz}, d_{yz})^4(d_{xy})^1$-type complexes. Consequently, the slope of the Curie plots for the *m*-H signal is positive. Therefore, the chemical shift and slope of the Curie plots of the *m*-H signal can tell the electronic ground state of the low-spin complexes.

Walker and co-workers proposed that the electronic ground state of low-spin iron(III) porphyrinates having *meso*-aryl groups such as $[Fe(TPP)L_2]^{\pm}$, $[Fe(OETPP)L_2]^{\pm}$, and $[Fe(TPC)L_2]^{\pm}$ (where TPC^{2-} = dianion of 5,10,15,20-tetraphenylchlorin) can be determined by the $\delta_m - \delta_p$ and $\delta_m - \delta_o$ values; δ_o, δ_m, and δ_p are the chemical shifts of the *o*-, *m*-, and *p*-phenyl signals, respectively.[2,3] If $\delta_m - \delta_p$ and $\delta_m - \delta_o$ are both large and positive, then the complex has large amounts of positive spin at the *meso*-C atoms, which, in turn, indicates that the complex adopts the $(d_{xz}, d_{yz})^4(d_{xy})^1$ ground state. In contrast, if $\delta_m - \delta_p$ and $\delta_m - \delta_o$ are small with $\delta_m - \delta_p$ positive and $\delta_m - \delta_o$ usually negative, then the complex adopts the $(d_{xy})^2(d_{xz}, d_{yz})^3$ ground state because the *meso*-C atoms have little or no spin density.

2. EPR Method. The electronic ground state of low-spin complexes can most clearly be determined by EPR spectroscopy, which is usually taken at extremely low temperatures. Complexes with the common $(d_{xy})^2(d_{xz}, d_{yz})^3$ ground state exhibit either rhombic or large g_{max}-type spectra depending on the orientation of the planar axial ligands.[2] If planar axial ligands such as imidazole and pyridine adopt a mutually parallel alignment above and below the porphyrin ring, the complexes exhibit the rhombic-type spectra. If, on the contrary, they adopt a mutually perpendicular alignment, the complexes exhibit single-feature large g_{max}-type spectra where a strong signal is observed at $g > 3.2$. Walker and co-workers revealed that the borderline between the parallel and perpendicular alignments is ca. 57°.[51] In contrast, complexes with the less common $(d_{xz}, d_{yz})^4(d_{xy})^1$ ground state exhibit the axial-type spectra where $g_{\perp}$ values are usually smaller than 2.5 and $g_{\parallel}$ values are 1.7−2.0.[2] If the energy level of the d_{xy} orbital is extensively higher than the energy levels of the $d_{\pi}(d_{xz}, d_{yz})$ orbitals, the complex adopts a quite pure $(d_{xz}, d_{yz})^4(d_{xy})^1$ ground state, where both $g_{\perp}$ and $g_{\parallel}$ values are close to 2.0.[2−8]

Electronic Ground State of 1. Figure 7 shows the Curie plots of the *o*-, *m*-, α-, *β*-, and *p*-$CH_2(\alpha)$ signals of series **1**. Each signal in **1a**−**1c** exhibits a considerable curvature. The results indicate that the $(d_{xz}, d_{yz})^4(d_{xy})^1$ ground state is destabilized at lower temperature. Thus, in the case of **1a**, the *m*-H signal (●, red) shows a slight downfield shift as the temperature is lowered from 313 to 273 K because **1a** adopts the $(d_{xz}, d_{yz})^4(d_{xy})^1$ ground state at ambient temperature. As the temperature is further lowered from 273 to 183 K, this signal is shifted to the opposite direction. The results are indicative of a gradual transition of the electronic ground state from $(d_{xz}, d_{yz})^4(d_{xy})^1$ to $(d_{xy})^2(d_{xz}, d_{yz})^3$. The *m*-H

dx.doi.org/10.1021/ic1024873 |*Inorg. Chem.* 2011, 50, 3567–3581

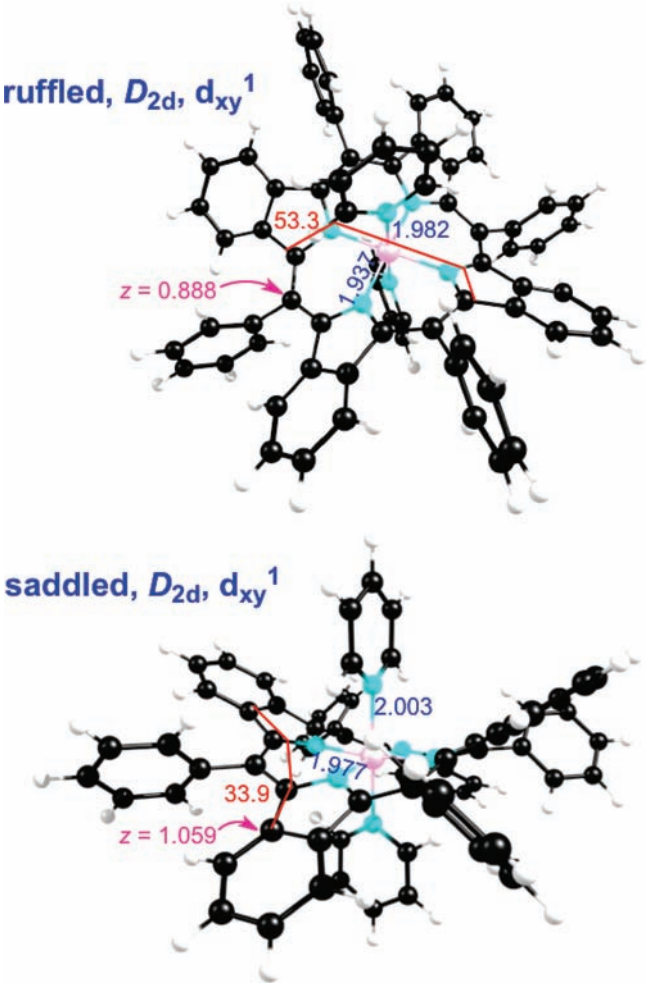

Figure 6. Structural highlights (Å, deg) of the ruffled and saddled $(d_{xz}, d_{yz})^4(d_{xy})^1$ states: Fe−N distances (in blue), displacements of selected atoms from the mean porphyrin plane (in magenta), and selected dihedrals (in red).

signals in **1b** and **1c** show a similar temperature dependence. In contrast, the Curie plots of the *m*-H signals in **1d** exhibit a good straight line with a positive slope, i.e., 1450 ppm·K. Similarly, **1e**, **1f**, and **1h** show a good straight line, as given in the Figure S5a of the SI; the slopes are 1500, 1520, and 1290 ppm·K, respectively. Furthermore, these lines intercept the axis of the ordinate at 7.17 (**1d**), 7.23 (**1e**), 7.39 (**1f**), and 6.83 (**1h**) ppm, which are close to the *m*-H chemical shift, 7.64 ppm, of the corresponding free-base porphyrin. Thus, **1d**−**1f** and **1h** maintain the $(d_{xz}, d_{yz})^4(d_{xy})^1$ ground state in the temperature range where the NMR spectra are taken. The signs of the Curie plots are also listed in Table 1.

Figure 8 demonstrates comparisons of the Curie plots of (a) *m*-H and (b) α-H signals in **1a**−**1f** and **1h**. Signals of **1a**−**1c** are signified by filled circles with red, blue, and green color, respectively. The Curie plots of all of the other complexes are given by the black symbols: **1d** (○), **1e** (□), **1f** (◇), and **1h** (△). In both the *m*-H and α-H signals, the curved lines change gradually to straight lines with positive slope as the axial ligand is changed from HIm (**a**) to 1-MeIm (**b**) and then to DMAP (**c**). Concomitantly, the curved line moves upward. The Curie plots of **1d**−**1f** and **1h** show almost overlapping straight lines although the Curie plots of the *m*-H signal of **1h** are located below those of **1d**−**1f** by 1−2 ppm.

Table 1 lists the $\delta_m - \delta_o$ values for **1**−**3**. All of the low-spin complexes in **1** exhibit $\delta_m - \delta_o$ values from 4.6 to 8.8 ppm at 298 K and from 5.1 to 12.2 ppm at 213 K. Close inspection of the data in Table 1 further indicates that the $\delta_m - \delta_o$ values increase on going from **1a**−**1c** to **1d**−**1f**. The results suggest that the spin densities at the meso positions in **1d**−**1f** are larger than those in **1a**−**1c**. It should be noted that the $\delta_m - \delta_o$ value of the DMAP complex (**1c**) is quite close to that of $[Fe(OETPP)(^tBuNC)_2]^+$ adopting the $(d_{xz}, d_{yz})^4(d_{xy})^1$ ground state; they are 5.49 and 5.51 ppm for **1c** and $[Fe(OETPP)(^tBuNC)_2]^+$, respectively, at 298 K.[22] These results strongly suggest that the d_{xy} orbital is located above the d_π orbitals even in the case of **1c**. Thus, it is clear that the TBzTArP core stabilizes the $(d_{xz}, d_{yz})^4(d_{xy})^1$ ground state as compared with the OETPP core.

The EPR spectra given in Figure 2 and *g* values listed in Table 2 are totally consistent with the NMR data. While **1a** and **1b** exhibit rhombic-type spectra characteristic of the $(d_{xy})^2(d_{xz}, d_{yz})^3$ ground state, **1d**−**1f** and **1h** show axial-type spectra characteristic of the $(d_{xz}, d_{yz})^4(d_{xy})^1$ ground state. The DMAP complex (**1c**) is the borderline case; the complex exhibits both the axial- and rhombic-type signals, showing the coexistence of electron configurational isomers even at 4.2 K.

DFT calculations of $[Fe(TBzTPP)(Py)_2]^+$ suggest that the $(d_{xz}, d_{yz})^4(d_{xy})^1$ state is more stable than the $(d_{xy})^2(d_{xz}, d_{yz})^3$ state for both the ruffled and saddled conformations. The dispersion-corrected calculations indicate that the ruffled conformation with the $(d_{xz}, d_{yz})^4(d_{xy})^1$ state is the most stable state, followed by the saddled conformation with the same state, as shown in Table 3. Because the energy difference between these states is quite small, it is reasonable to consider an equilibrium between these two isomers, as indicated by eq 4, where d_{xy}^1 indicates the $(d_{xz}, d_{yz})^4(d_{xy})^1$ ground state.

$$\text{saddled}(d_{xy}^1) \rightleftarrows \text{ruffled}(d_{xy}^1) \quad (4)$$

The observed chemical shift (δ_{obs}) for the *m*-H signal can be expressed by eq 5, where p is the population ratio of the saddled isomer and δ(saddled) and δ(ruffled) are the *m*-H chemical shifts of each isomer. The first term in eq 5 should be negative (upfield shift) because the Mulliken spin population of *m*-C in the saddled complex (state C in Table 4) is slightly positive. However, the second term should be positive (downfield shift) because the corresponding Mulliken spin-population value in the ruffled complex (state A in Table 4) is slightly negative.

$$\delta_{obs} = p(\text{saddled})\cdot\delta(\text{saddled}) + p(\text{ruffled})\cdot\delta(\text{ruffled}) \quad (5)$$

The observed chemical shift for the *m*-H signal of structurally analogous $[Fe(TBzTArP)(Py)_2]^+$ (**1f**) is 12.48 ppm at 298 K, which can be explained if the second term in eq 5 is predominant. The straight line in the Curie plots suggests that the equilibrium constant corresponding to eq 4 is invariant throughout the NMR measurement.

On the basis of these results, we concluded that *all of the complexes of* **1** *adopt the* $(d_{xz}, d_{yz})^4(d_{xy})^1$ *ground state at least at ambient temperature regardless of the kinds of axial ligands*. As the temperature is lowered, the electronic ground state gradually changes from $(d_{xz}, d_{yz})^4(d_{xy})^1$ to $(d_{xy})^2(d_{xz}, d_{yz})^3$ in the cases of **1a**−**1c**. At an extremely low temperature, both **1a** and **1b** adopt the $(d_{xy})^2(d_{xz}, d_{yz})^3$ ground state, while **1c** exists as an equilibrium mixture of two electron configurational isomers, as revealed from the EPR spectra. In contrast, all the other complexes, **1d**−**1f**

dx.doi.org/10.1021/ic1024873 |*Inorg. Chem.* 2011, 50, 3567–3581

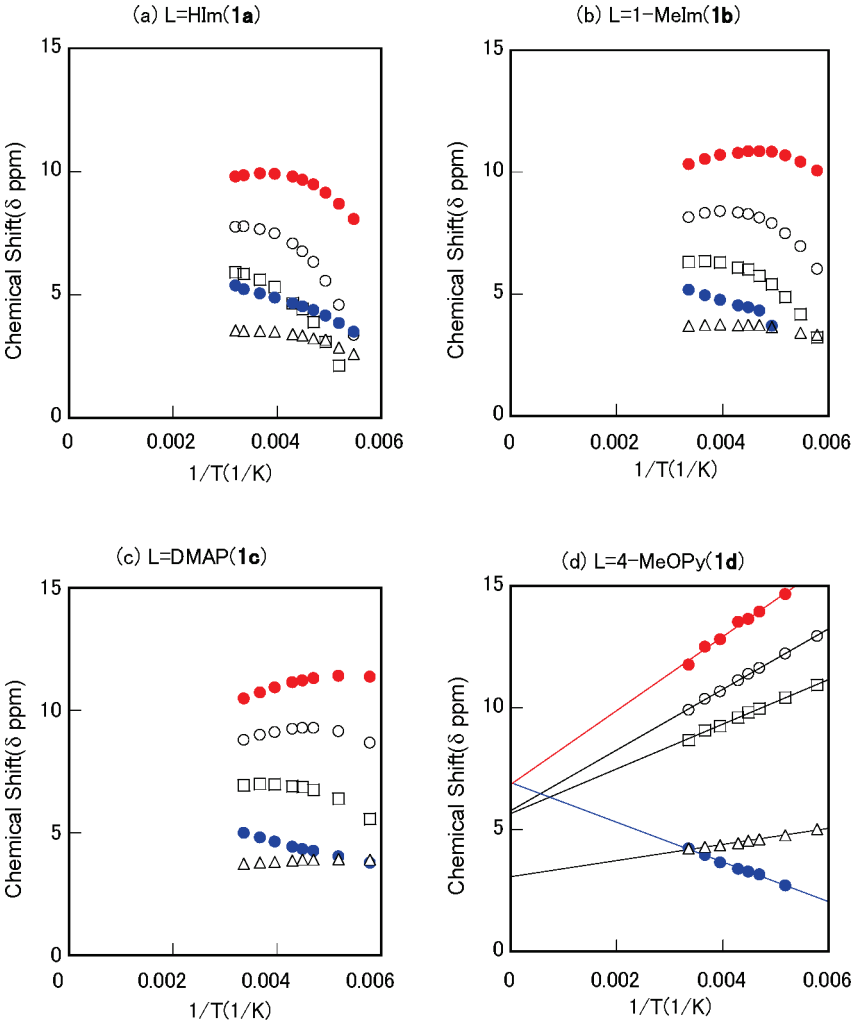

Figure 7. Curie plots of some signals in **1a**−**1d**, where the symbols of blue ●, red ●, ○, □, and Δ show the chemical shifts of *o*-, *m*-, α-, *β*-, and *p*-CH_2, respectively.

and **1h**, maintain the $(d_{xz}, d_{yz})^4(d_{xy})^1$ ground state from 298 to 4.2 K. Therefore, the stability of the $(d_{xz}, d_{yz})^4(d_{xy})^1$ ground state increases as the axial ligand changes from HIm to Py in the order given as follows:

$$\text{HIm} < \text{1-MeIm} < \text{DMAP} < \text{4-MeOPy} < \text{4-MePy} < \text{Py},\ \text{CN}^-$$

It should be noted that the $(d_{xz}, d_{yz})^4(d_{xy})^1$ ground state observed in the HIm complex (**1a**) at ambient temperature is quite unusual because almost all of the previously reported HIm complexes exhibit the $(d_{xy})^2(d_{xz}, d_{yz})^3$ ground state. The result suggests that the stability of the $(d_{xz}, d_{yz})^4(d_{xy})^1$ ground state is an inherent characteristic of the TArTBzP core.

The reason for the stability of the less common $(d_{xz}, d_{yz})^4(d_{xy})^1$ state in **1** can be expressed as follows. As suggested by DFT calculations, $[Fe(TBzTPP)(Py)_2]^+$ appears to exist as an equilibrium mixture of two conformers with the $(d_{xz}, d_{yz})^4(d_{xy})^1$ ground state. In the saddled conformation, there is a strong interaction between the iron d_{xy} and porphyrin a_{1u} orbitals, as revealed from the large Mulliken spin population of the C_α atoms, i.e., 0.0900, together with the exceedingly small spin population of the Fe atom, i.e., 0.3307. The interaction destabilizes the d_{xy} orbital and places it above the d_π orbitals. In the ruffled conformer, the d_{xy} orbital should also be destabilized relative to the d_π orbitals because of interaction with the porphyrin a_{2u} orbital, as revealed from the large Mulliken spin population of the *meso*-C atoms, i.e., 0.0878. In addition, the d_π orbitals of both conformers can be stabilized by bonding interaction with the low-lying LUMO of the TArTBzP ring, which is further verified by the bathochromic shifts of the absorption bands in TBzTArP, as compared with the corresponding TBuTArP shown in Figure S6a,b of the SI.

Electronic Ground State of 2. The Curie plots of series **2** given in Figures 9 and 10 are instructive. While the Curie plots of the *m*-H signals of **1a**−**1c** exhibit a curvature as shown in Figures 7, 8, and S5b of the SI, those of **2a**−**2c** show straight lines with negative slopes; they are −480, −530, and −1030 ppm·K, respectively. Negative slopes are also observed in the Curie plots of the *m*-H signals in other typical low-spin complexes with the $(d_{xy})_2(d_{xz}, d_{yz})^3$ ground state such as $[Fe(OETPP)(HIm)_2]^+$ and $[Fe(TPP)(HIm)_2]^+$; they are −1200 and −490 ppm·K, respectively.[22,52] By contrast, the Curie plots of the *m*-H signals in **2d**−**2f** and **2h** exhibit reasonably good straight lines with positive slopes; they are +550, +890, +1340, and +900 ppm·K, respectively. These values are only 37−88% of the corresponding values of **1d**−**1f** and **1h**. Furthermore, the

dx.doi.org/10.1021/ic1024873 |*Inorg. Chem.* 2011, 50, 3567–3581

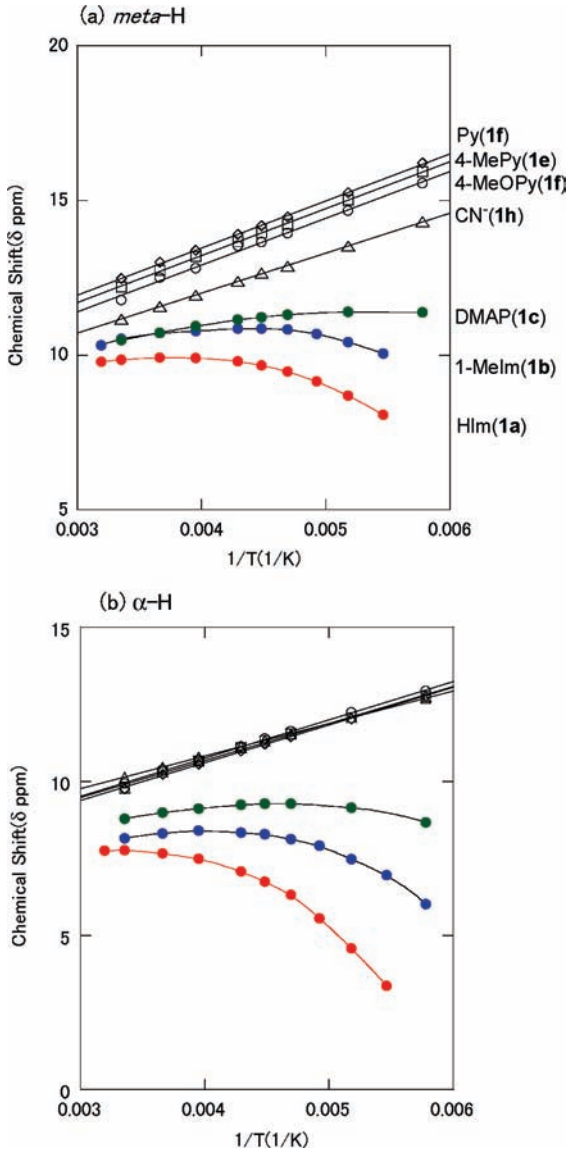

Figure 8. Curie plots of the *m*-H (a) and α-H (b) signals of **1a**−**1f** and **1h**.

$\delta_m - \delta_o$ values are 3.87 (**2d**), 4.85 (**2e**), 6.19 (**2f**), and 4.77 (**2h**) ppm at 213 K, which are again much smaller than those of **1d**−**1f** and **1h**; they are 10.8, 11.5, 12.2, and 8.6 ppm, respectively, at the same temperature. Thus, it is reasonable to conclude that **2a**−**2c** are in the $(d_{xy})^2(d_{xz}, d_{yz})^3$ ground state. In contrast, **2d**−**2f** and **2h** are in the $(d_{xz}, d_{yz})^4(d_{xy})^1$ ground state although the energy gaps between the d_{xy} and d_π orbitals in these complexes are much smaller than those in **1d**−**1f** and **1h**. The Curie plot of the *m*-H signal of the 4-CNPy complex (**2g**) is quite unique. A considerably large curvature can be explained in terms of the spin transition from $S = {}^3/_2$ to $S = {}^1/_2$ with the $(d_{xz}, d_{yz})^4(d_{xy})^1$ ground state. Note that the *m*-H signal of the pure $S = {}^3/_2$ complex, $[Fe(OETPP)(4\text{-}CNPy)_2]^+$, appears at 5.27 ppm at 298 K, which is shown in Figure 10a by the symbol indicated by the arrow.[2]

Interestingly, the Curie plots of the α-CH_2 signals in all of the complexes, **2a**−**2h**, exhibit more or less a curvature, as shown in Figure 10b. Among these complexes, **2a**−**2c** show straight lines at least below 250 K. Thus, they adopt the $(d_{xy})^2(d_{xz}, d_{yz})^3$ ground state although the population of $S = {}^3/_2$ is not zero at 298 K. Similarly, **2h** shows a reasonably good linearity throughout the temperature range examined, suggesting that the complex maintains the $(d_{xz}, d_{yz})^4(d_{xy})^1$ ground state. In contrast to these complexes, the curvature of the α-CH_2 signals increases gradually on going from **2d** to **2f**, suggesting that the population of $S = {}^3/_2$ increases at higher temperature in this order. It should be noted, however, that the $S = {}^3/_2$ populations in **2d**−**2f** are still not predominant even at 298 K because the chemical shifts of the α-CH_2 signals of these complexes are ca. 30 ppm compared with the corresponding chemical shift, 88.6 ppm, of the pure $S = {}^3/_2$ complex, i.e., $[Fe(TBTXP)(THF)_2]^+$ (where THF = tetrahydrofuran).[53] The curvature observed in the α-CH_2 signals of **2d**−**2f**, although it is not observed in the *m*-H signals of the same complexes, can be explained in terms of the large differences in the chemical shifts between the $(d_{xz}, d_{yz})^4(d_{xy})^1$ and $S = {}^3/_2$ complexes. Thus, the α-CH_2 signal is a sensitive probe of the detailed electronic structure of **2**. The spin transition is most explicitly observed in **2g**, which exhibits the α-CH_2 signal at an extremely downfield position, 49.8 ppm, at 273 K. The result indicates that **2g** exists mainly as $S = {}^3/_2$ at ambient temperature, like $[Fe(OETPP)(4\text{-}CNPy)_2]^+$. This signal moves upfield upon a decrease in the temperature and approaches that of **2h** at 213 K, as shown in Figure 10b, suggesting that the complex is $S = {}^1/_2$ (d_{xy}) at this temperature.

EPR spectra shown in Figure 2B are totally consistent with the conclusion obtained by the NMR spectra. The complexes **2a** and **2b** exhibit rhombic-type spectra, while **2d**−**2h** exhibit axial-type spectra. Thus, the former complexes maintain the $(d_{xy})^2(d_{xz}, d_{yz})^3$ ground state, while the latter complexes maintain the $(d_{xz}, d_{yz})^4(d_{xy})^1$ ground state in the temperature range 298−4.2 K. In the case of **2c**, very broad unresolved signals are observed at $g = 3.0-2.3$. Presumably, the two low-field signals in the rhombic-type spectrum overlap because of poor resolution. The data in Table 2 indicate that the $g_\perp$ values of **2d**−**2h** are larger than those of the corresponding **1d**−**1h**. The results suggest that the energy gap between the d_{xy} and d_π orbitals for **1d**−**1h** is larger than that for the corresponding complexes **2d**−**2h**. A direct comparison of the tetragonal splitting is only possible for **1 h′** and **2h′**. As expected, the former is -6.3λ, while the latter is -4.0λ.

On the basis of these results, we concluded that, *while* ***2a***−***2c*** *and* ***2h*** *adopt the* $(d_{xy})^2(d_{xz}, d_{yz})^3$ *and* $(d_{xz}, d_{yz})^4(d_{xy})^1$ *ground states, respectively, throughout the temperature range examined by NMR and EPR spectroscopy,* ***2d***−***2f*** *exhibit spin transition from the mixed* $S = {}^3/_2, {}^1/_2$ *state to the mixed* $(d_{xy})^2(d_{xz}, d_{yz})^3$ *and* $(d_{xz}, d_{yz})^4(d_{xy})^1$ *state as the temperature is lowered from 298 to 173 K. These complexes are finally converted to the* $(d_{xz}, d_{yz})^4(d_{xy})^1$ *state as the temperature is further lowered to 4.2 K. In the case of* ***2g****, spin transition occurs from the nearly pure* $S = {}^3/_2$ *to the nearly pure* $(d_{xz}, d_{yz})^4(d_{xy})^1$*state.* Similar spin transitions have been observed in structurally similar $[Fe(OETPP)(Py)_2]^+$ (**3f**), $[Fe(OMTPP)L_2]^+$ (L = 4-CNPy and Py, where $OMTPP^{2-}$ = dianion of 2,3,7,8,12,13,17,18-octamethyl-5,10,15,20-tetraphenylporphyrin), and $[Fe(TBTXP)L_2]^+$ (L = 4-CNPy and Py).[53]

Because the six-coordinate, low-spin $[Fe(TPP)L_2]^\pm$ and $[Fe(OEP)L_2]^\pm$ complexes adopt the $(d_{xy})^2(d_{xz}, d_{yz})^3$ ground state at 4.2 K if the axial ligands are those examined in this study except for 4-CNPy, it is concluded on the basis of the present work together with our previous work that stabilization of the $(d_{xz}, d_{yz})^4(d_{xy})^1$ ground state in low-spin $[Fe(Por)L_2]^\pm$ increases in the order given below (where T^iPrP^{2-} = dianion of 5,10,15,20-tetraisopropylporphyrin):[22]

OETPP, OEP < OMTPP, TPP < TBuTArP < TBzTArPy < T^iPrP

dx.doi.org/10.1021/ic1024873 |*Inorg. Chem.* 2011, 50, 3567–3581

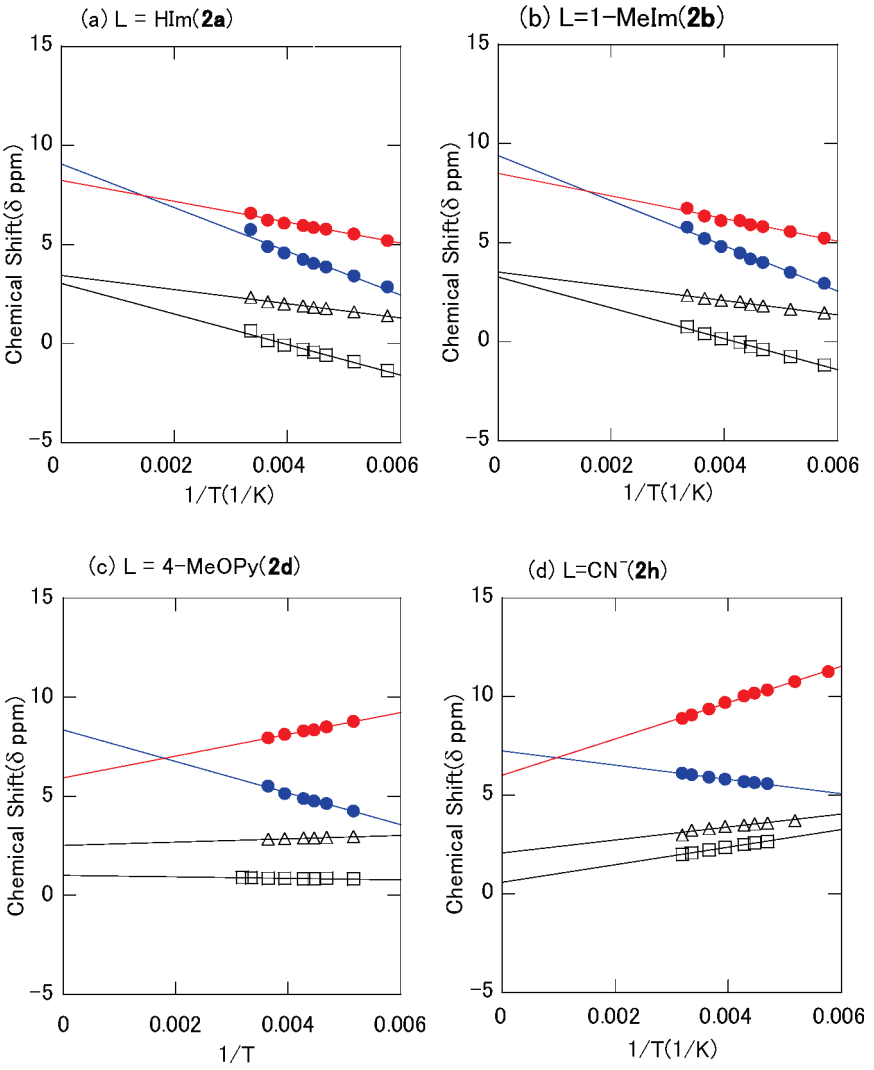

Figure 9. Curie plots of some signals in **2a**, **2b**, **2d**, and **2h**, where the symbols of blue ●, red ●, □, and Δ show the chemical shifts of *o*-, *m*-, *β*-, and *p*-CH_2, respectively.

■ CONCLUSION

The electronic structures of low-spin, six-coordinate **1** and **2**, where the axial ligands (L) are HIm, 1-MeIm, DMAP, 4-MeOPy, 4-MePy, Py, and CN^-, were examined by ^1H NMR and EPR spectroscopy as well as DFT calculation. These complexes were classified into two groups. Group A consists of complexes having strong σ donors such as HIm, 1-MeIm, and DMAP as axial ligands, and group B consists of complexes having 4-MeOPy, 4-MePy, Py, and CN^- as axial ligands. In the case of **1**, the group A complexes switch the electronic ground state from $(d_{xz}, d_{yz})^4(d_{xy})^1$ at ambient temperature to $(d_{xy})^2(d_{xz}, d_{yz})^3$ at 4.2 K; the DMAP complex exists as a mixture of two kinds of electron configurational isomers even at 4.2 K. The group B complexes maintained the $(d_{xz}, d_{yz})^4(d_{xy})^1$ ground state in a wide temperature range, i.e., 298−4.2 K. DFT calculations were carried out on different conformations and electronic states of $[Fe(TBzTPP)(Py)_2]^+$. The calculations including Grimme's dispersion corrections (BP86-D and BLYP-D) indicated that the ruffled conformation with the $(d_{xz}, d_{yz})^4(d_{xy})^1$ state is the most stable state, followed by the saddled conformation with the same state. The complex is unique in that the highly ruffled and highly saddled conformers are almost identical in energy. Thus, the group B complexes are supposed to exist as an equilibrium mixture of the two conformers with the $(d_{xz}, d_{yz})^4(d_{xy})^1$ ground state. In sharp contrast to **1**, the group A complexes in **2** maintained the $(d_{xy})^2(d_{xz}, d_{yz})^3$ ground state throughout the temperature range examined, i.e., 298−4.2 K. Although the group B complexes in **2** maintained the $(d_{xz}, d_{yz})^4(d_{xy})^1$ ground state as in the case of **1**, the energy gaps between the d_{xy} and d_π orbitals are much smaller than those in **1**. DFT calculations suggested that the stability of the $(d_{xz}, d_{yz})^4(d_{xy})^1$ ground state of **1** may be ascribed to the strong interaction between the iron d_{xy} and the high-energy a_{1u} HOMO, which is an inherent characteristic of the saddled TBzTArP core. In addition, the ruffled conformer shows a $d_{xy}-a_{2u}$ interaction, which is quite common in low-spin iron(III) porphyrinates with a ruffled porphyrin core. The presence of a low-lying LUMO, which is also an inherent characteristic of the TBzTArP core, should also contribute to stabilization of the $(d_{xz}, d_{yz})^4(d_{xy})^1$ ground state via $d_\pi-p_\pi^*$ interactions. On the basis of these results, we concluded that benzoannelation of porphyrin stabilizes the $(d_{xz}, d_{yz})^4(d_{xy})^1$ ground state in low-spin iron(III) porphyrinates.

dx.doi.org/10.1021/ic1024873 |*Inorg. Chem.* 2011, 50, 3567–3581

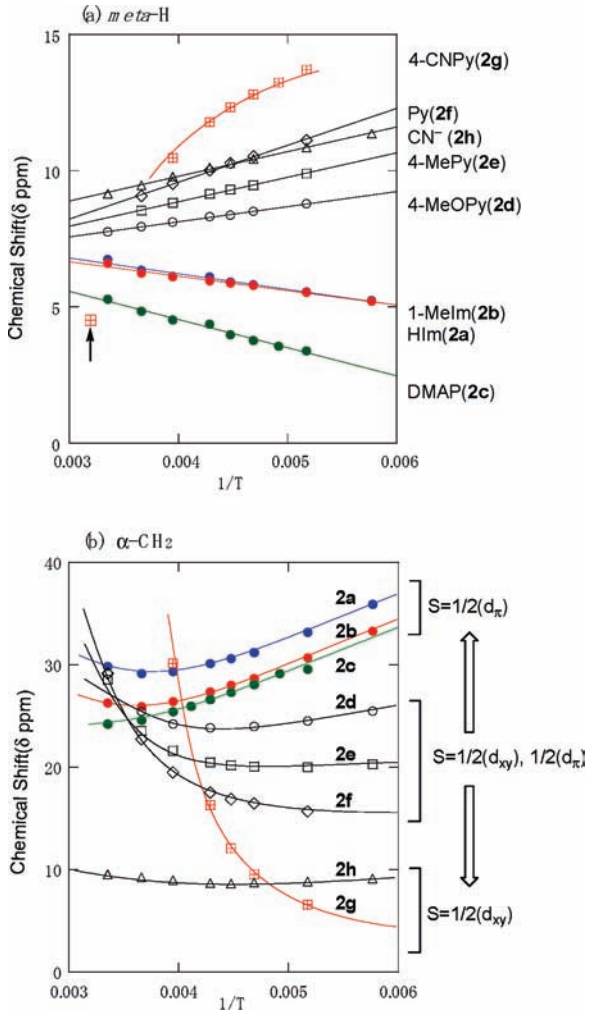

Figure 10. Curie plots of the (a) *m*-H and (b) α-CH_2 signals of **2**. The symbol indicated by the arrow in part a indicates the *m*-H signal of $[Fe(OETPP)(THF)_2]^+$ with a pure intermediate-spin state.

EXPERIMENTAL SECTION

General Procedure. NMR samples of six-coordinate complexes, $[Fe(TBzTArP)(L)_2]^{\pm}$ and $[Fe(TBuTArP)(L)_2]^{\pm}$, were prepared by the direct addition of an excess (5−10 equiv) of the desired axial ligand to CD_2Cl_2 solutions of Fe(TBzTArP)Cl and Fe(TBuTArP)Cl placed in 5 mm NMR sample tubes. ^{1}H NMR spectra were recorded on a JEOL LA 300 or LA400 spectrometer operating at 300.4 and 400.6 MHz, respectively, and referenced to the resonance of the residual solvent protons of CD_2Cl_2 (δ = 5.32 ppm relative to tetramethylsilane). UV−vis spectra were recorded in CH_2Cl_2 solutions at room temperature using a Shimazu UV-3100 spectrophotometer. EPR spectra were measured at 4.2−17.0 K on a Bruker E500 spectrometer operating at X band and equipped with an Oxford helium cryostat. Samples for EPR measurement were similarly prepared in 5 mm EPR tubes as mentioned for NMR measurement. The concentrations of the EPR samples were 5−8 mM. The time-of-flight mass spectra were recorded on a Bruker Daltonics autoflex-T1 mass spectrometer.

Synthesis[54]. *2:3,7:8,12:13,17:18-Tetrabutano-5,10,15,20-tetrakis-(4-nonylphenyl)porphyrin, TBuTArPH$_2$.* 3:4-Butanopyrrole (1.66 g, 1.37 mmol) and 4-nonylbenzaldehyde (0.31 g, 1.37 mmol) were dissolved in dry, freshly distilled CH_2Cl_2 (137 mL). The solution was stirred at room temperature under a slow steady stream of argon for 15 min. The flask was shielded from light, and $BF_3 \cdot OEt_2$ (0.02 mL, 0.137 mmol) was added. The resulting solution, after stirring for 1 h at room temperature, was treated with dichlorodicyanoquinone (DDQ; 1.30 g, 6.60 mmol) and then was refluxed under argon for 1 h to give a dark-green solution. The solvent was removed under vacuum, and the residue was purified by column chromatography on alumina (grade III) using CH_2Cl_2 as the eluent. Recrystallization from methanol gave TBuTArPH$_2$ (0.18 g, 56%) as purple crystals. ^{1}H NMR (300 MHz, $CDCl_3$): δ 8.11−8.08, (d, 8H, J = 7.7 Hz, *o*-Ar), 7.52−7.49 (d, 8H, J = 7.8 Hz, *m*-Ar), 2.97−2.92 (t, 8H, each, CH_2), 2.33−1.29 (m, 40H, CH_2), 0.94−0.92 (t, 12H, CH_3). UV−vis [CH_2Cl_2; λ_{max}, nm (ε, M^{-1} cm^{-1})]: 446 (66 084), 542 (5052), 615 (3720), 679 (5698). MS (MALDI): m/z 1335.30 (M^+). Anal. Calcd for $C_{96}H_{126}N_4$: C, 84.03; H, 9.56; N, 4.09. Found: C, 84.23; H, 9.35; N, 4.24. ^{13}C NMR (300 MHz, $CDCl_3$): δ 144. 1, 140.7, 136.2, 129.1, 118.5, 37.4, 33.5, 33.1, 31.29, 31.24, 30.97, 30.64, 27.3, 25.1, 24.2, 15.7.

2:3,7:8,12:13,17:18-Tetrabenzo-5,10,15,20-tetrakis(4-nonylphenyl)-porphyrin, TBzTArPH$_2$. To a toluene (20 mL) solution of TBuTArPH$_2$ (150 mg, 0.12 mmol) was added an excess of copper(II) chloride (162 mg, 1.2 mmol). The mixture was refluxed for 2 h, and then the solvent was evaporated under vacuum. The resulting residue was dissolved in CH_2Cl_2 (150 mL) and washed once with a saturated aqueous $NaHCO_3$ solution and once with water. The organic layer, after drying over anhydrous Na_2SO_4, was removed under vacuum. The remaining residue was purified by column chromatography on alumina using CH_2Cl_2 as the eluent. A toluene solution (20 mL) of purple Cu(TBuTArP) (109 mg, 0.78 mmol) was treated with excess DDQ (176 mg, 7.9 mmol), and the resulting mixture was refluxed for 5 min. The color changed from red to deep green during the reflux. The reaction mixture was cooled to room temperature, diluted with $CHCl_3$ (100 mL), and washed once with a saturated aqueous $NaHCO_3$ solution and once with water. The solvent was removed under vacuum, and the remaining residue was purified by column chromatography on alumina using $CHCl_3$ as the eluent. Recrystallization from methanol afforded Cu(TBzTArP) (65 mg, 60% yield) as a dark-green solid. Cu(TBzTArP) (60 mg, 0.043 mmol) was dissolved in concentrated H_2SO_4 and stirred for 5 min at room temperature. The acid solution was poured into water and extracted repeatedly with $CHCl_3$ until the organic extracts were colorless. The combined organic layers, after drying over anhydrous Na_2SO_4, were concentrated under vacuum. Recrystallization from methanol gave green crystals of TBzTArPH$_2$ (45 mg, 79% yield). ^{1}H NMR ($CDCl_3$, 298 K): δ 8.22 (d, J = 7.60 Hz, 8H, *o*-H), 7.64 (d, J = 7.60 Hz, 8H, *m*-H), 7.38−7.09 (br m, 16H, benzo-H), 3.03 (t, J = 7.60 Hz, 8H, *p*-CH_2), 1.95 (m, 8H, *p*-CH_2), 1.66−1.28 (m, 48H, *p*-$(CH_2)_6$), 0.91 (t, J = 6.8 Hz, 12H, *p*-CH_3), −1.22 (s, 2H, NH). UV−vis [CH_2Cl_2; λ_{max}, nm (ε, M^{-1} cm^{-1})]: 461 (458 000), 503 (31 900), 589 (18 000), 641 (49 600), 695 (11 300) nm. MS (MALDI-TOF). Calcd for $C_{96}H_{110}N_4$: m/z 1319.9. Found: m/z 1319.6.

Fe(TBzTArP)Cl and Fe(TBuTArP)Cl. Insertion of iron(III) into TBzTArPH$_2$ and TBuTArPH$_2$ was carried out by the addition of $FeCl_2 \cdot 6H_2O$ into a refluxed *N*,*N*-dimethylformamide solution of TBzTArPH$_2$ and TBuTArPH$_2$. The UV−vis spectra of these complexes are given in Figure S6a of the SI.

[Fe(TBzTArP)(THF)$_2$]BF$_4$ and [Fe(TBuTArP)(THF)$_2$]BF$_4$. These complexes were prepared by the addition of $AgBF_4$ to a THF solution of Fe(TBzTArP)Cl and Fe(TBuTArP)Cl, respectively, followed by recrystallization from CH_2Cl_2/hexane.

[Fe(TBzTArP)(L)$_2$]Cl and [Fe(TBuTArP)(L)$_2$]Cl (L = HIm, 1-MeIm, DMAP, 4-MeOPy, 4-MePy, and Py). NMR samples of these complexes were prepared by the addition of the CD_2Cl_2 solutions of various axial ligands (L) mentioned above to the CD_2Cl_2 solutions of Fe(TBzTArP)Cl and Fe(TBuTArP)Cl. As the ligands were added, the ^{1}H NMR spectra showed a drastic change. The ligand solutions were added until no spectral change was observed.

[Fe(TBzTArP)(CN)$_2$](Bu$_4$N) and [Fe(TBuTArP)(CN)$_2$](Bu$_4$N). These complexes were similarly prepared by the addition of the CD_2Cl_2

solution of tetrabutylammonium cyanide ($Bu_4N^+CN^-$) to the CD_2Cl_2 solutions of Fe(TBzTArP)Cl and Fe(TBuTArP)Cl. The UV−vis spectra of $[Fe(TBzTArP)(CN)_2](Bu_4N)$ and $[Fe(TBuTArP)(CN)_2](Bu_4N)$ are given in Figure S6b of the SI.

[Fe(TBuTArP)(4-CNPy)$_2$]BF$_4$. Complete formation of the bis(4-CNPy) complex was confirmed when a large excess (ca. 40 equiv) of 4-CNPy was added to the CD_2Cl_2 solution of $[Fe(TBuTArP)(THF)_2]BF_4$. However, the corresponding $[Fe(TBzTArP)(4\text{-}CNPy)_2]BF_4$ was not formed even by the addition of 60 equiv of 4-CNPy to the CD_2Cl_2 solution of $[Fe(TBzTArP)(THF)_2]BF_4$.

DFT Calculations. All calculations were carried out with the *ADF 2009* program system. An STO-TZP basis set, as well as fine meshes for numerical integration of matrix elements and tight criteria for geometry optimization, was used throughout. Calculations were carried out with a number of functionals including BP86, BLYP, and OLYP. Classic pure functionals such as BP86 and BLYP often yield somewhat better geometries for transition-metal complexes, whereas the newer pure functional OLYP and hybrid functionals such as B3LYP sometimes overestimate metal−ligand distances, even though the latter generally yield better energetics.[55] In this case, all of the functionals examined (BP86, BLYP, and OLYP) gave very similar geometries, Mulliken charges, and spin populations. Including Grimme's dispersion corrections (such as BP86-D and BLYP-D) resulted in some modulation of the ruffling and saddling dihedrals as well as the relative energetics of the different states.

■ ASSOCIATED CONTENT

Supporting Information. ^{1}H NMR, COSY, EPR, and UV−vis spectra and Curie plots. This material is available free of charge via the Internet at http://pubs.acs.org.

■ AUTHOR INFORMATION

Corresponding Author

*E-mail: ikeue@riko.shimane-u.ac.jp (T.I.), abhik@chem.uit.no (A.G.), vicente@lsu.edu (M.G.H.V.), mnakamu@med.toho-u.ac.jp (M.N.).

■ ACKNOWLEDGMENT

This work was supported by Grants-in-Aid for Scientific Research from the Ministry of Education, Culture, Sports, Science and Technology, Japan (Grant 22750052 to T.I. and Grant 22550157 to M.N.). A.G. was supported by the Research Council of Norway. M.N. thanks the Research Center for Materials with Integrated Properties, Toho University, for financial support. Thanks are due to the Research Center for Molecular-Scale Nanoscience, the Institute for Molecular Science.

■ REFERENCES

(1) Scheidt, W. R. In *The Porphyrin Handbook*; Kadish, K. M., Smith, K. M., Guilard, R., Eds.; Academic Press: San Diego, CA, 2000; Vol. 3, Chapter XX, pp 49−112.

(2) Walker, F. A. In *The Porphyrin Handbook*; Kadish, K. M., Smith, K. M., Guilard, R., Eds.; Academic Press: San Diego, CA, 2000; Vol. 5, Chapter 36, pp 81−183.

(3) Walker, F. A. *Inorg. Chem.* **2003**, *42*, 4526–4544.

(4) Walker, F. A. *Chem. Rev.* **2004**, *104*, 589–616.

(5) Nakamura, M. *Coord. Chem. Rev.* **2006**, *250*, 2271–2294.

(6) Nakamura, M.; Ohgo, Y.; Ikezaki, A. *J. Inorg. Biochem.* **2008**, *102*, 433–445.

(7) Ikezaki, A.; Ohgo, Y.; Nakamura, M. *Coord. Chem. Rev.* **2009**, *253*, 2056–2069.

(8) Nakamura, M.; Ohgo, Y.; Ikezaki, A. . In *Handbook of Porphyrin Science*; Kadish, K. M., Smith, K. M., Guilard, R., Eds.; World Scientific: Singapore, 2010; Vol. 7, pp 1−146.

(9) Safo, M. K.; Gupta, G. P.; Watson, C. T.; Simonis, U.; Walker, F. A.; Scheidt, W. R. *J. Am. Chem. Soc.* **1992**, *114*, 7066–7075.

(10) Safo, M. K.; Walker, F. A.; Raitsimring, A. M.; Walters, W. P.; Dolata, D. P.; Debrunner, P. G.; Scheidt, W. R. *J. Am. Chem. Soc.* **1994**, *116*, 7760–7770.

(11) Cheesman, M. R.; Walker, F. A. *J. Am. Chem. Soc.* **1996**, *118*, 7373–7380.

(12) Walker, F. A.; Nasri, H.; Turowska-Tyrk, I.; Mohanrao, K.; Watson, C. T.; Shokhirev, N. V.; Debrunner, P. G.; Scheidt, W. R. *J. Am. Chem. Soc.* **1996**, *118*, 12109–12118.

(13) Simonneaux, G.; Schünemann, V.; Morice, C.; Carel, L.; Toupet, L.; Winkler, H.; Trautwein, A. X.; Walker, F. A. *J. Am. Chem. Soc.* **2000**, *122*, 4366–4377.

(14) Nakamura, M.; Ikeue, T.; Fujii, H.; Yoshimura, T. *J. Am. Chem. Soc.* **1997**, *119*, 6284–6291.

(15) Wołowiec, S.; Latos-Grażyński, L.; Mazzanti, M.; Marchon, J.-C. *Inorg. Chem.* **1997**, *36*, 5761–5771.

(16) Wojaczynski, J.; Latos-Grazynski, L.; Glowiak, T. *Inorg. Chem.* **1997**, *36*, 6299–6306.

(17) Pilard, M.-A.; Guillemot, M.; Toupet, L.; Jordanov, J.; Simonneaux, G. *Inorg. Chem.* **1997**, *36*, 6307–6314.

(18) Wojaczynski, J.; Latos-Grazynski, L.; Toronto, D.; Marchon, J.-C. *Inorg. Chem.* **1998**, *37*, 724–732.

(19) Nakamura, M.; Ikeue, T.; Fujii, H.; Yoshimura, T.; Tajima, K. *Inorg. Chem.* **1998**, *37*, 2405–2414.

(20) Nakamura, M.; Ikeue, T.; Ikezaki, A.; Ohgo, Y.; Fujii, H. *Inorg. Chem.* **1999**, *38*, 3857–3862.

(21) Ikeue, T.; Ohgo, Y.; Saitoh, T.; Nakamura, M.; Fujii, H.; Yokoyama, M. *J. Am. Chem. Soc.* **2000**, *122*, 4068–4076.

(22) Ikeue, T.; Ohgo, Y.; Saitoh, T.; Yamaguchi, T.; Nakamura, M. *Inorg. Chem.* **2001**, *40*, 3423–3434.

(23) Ema, T.; Senge, M. O.; Nelson, N. Y.; Ogoshi, H.; Smith, K. M. *Angew. Chem., Int. Ed.* **1994**, *33*, 1879–1881.

(24) Jentzen, W.; Simpson, M. C.; Hobbs, J. D.; Song, X.; Ema, T.; Nelson, N. Y.; Medforth, C. J.; Smith, K. M.; Veyrat, M.; Ramasseul, R.; Marchon, J.-C.; Takeuchi, T.; Goddard, W. A.; Shelnutt, J. A. *J. Am. Chem. Soc.* **1995**, *117*, 11085–11097.

(25) Senge, M. O.; Ema, T.; Smith, K. M. *J. Chem. Soc., Chem. Commun.* **1995**, 733–734.

(26) Veyrat, M.; Ramasseul, R.; Marchon, J.-C.; Turowska-Tyrk, I.; Scheidt, W. R. *New J. Chem.* **1995**, *19*, 1199–1202.

(27) Mazzanti, M.; Veyrat, M.; Ramasseul, R.; Marchon, J.-C.; Turowska-Tyrk, H.; Shang, M.; Scheidt, W. R. *Inorg. Chem.* **1996**, *35*, 3733–3734.

(28) Conradie, J.; Ghosh, A. *J. Phys. Chem. B* **2003**, *107*, 6486–6490.

(29) Cheng, R.-J.; Chen, P.-Y.; Lovell, T.; Liu, T.; Noodleman, L.; Case, D. A. *J. Am. Chem. Soc.* **2003**, *125*, 6774–6783.

(30) Ikeue, T.; Ohgo, Y.; Yamaguchi, T.; Takahashi, M.; Takeda, M.; Nakamura, M. *Angew. Chem., Int. Ed.* **2001**, *40*, 2617–2620.

(31) Taylor, C. P. S. *Biochim. Biophys. Acta* **1977**, *491*, 137–149.

(32) Palmer, G. . In *Iron Porphyrins*; Part, I. I., Lever, A. B. P., Gray, H. B., Eds.; Physical Bioinorganic Chemistry Series 2; Addison-Wesley: Reading, MA. 1983; pp 43−88.

(33) Walker, F. A. *Coord. Chem. Rev.* **1999**, *185−186*, 471–534.

(34) Ghosh, A. In *The Porphyrin Handbook*; Kadish, K. M., Guilard, R., Smith, K. M., Eds.; Academic Press: New York, 1999; Vol. 7, pp 1−38.

(35) Ghosh, A.; Gonzalez, E.; Vangberg, T. *J. Phys. Chem. B* **1999**, *103*, 1363–1367.

(36) Cheng, R.-J.; Chen, P.-Y. *Chem.—Eur. J.* **1999**, *5/6*, 1708–1715.

(37) Cheng, R.-J.; Wang, Y.-K.; Chen, P.-Y.; Han, Y.-P.; Chang, C.-C. *Chem. Commun.* **2005**, 1312.

(38) Cheng, R.-J.; Chao, C.-W.; Han, Y.-P.; Chen, Y.-C.; Ting, C.-H. *Chem. Commun.* **2009**, 2180–2182.

(39) The OPTX exchange functional: Handy, N. C.; Cohen, A. *J. Mol. Phys.* **2001**, *99*, 403–412.

(40) The LYP correlation functional: Lee, C.; Yang, W.; Parr, R. G. *Phys. Rev.* **1988**, *B37*, 785–789.
(41) Becke, A. D. *Phys. Rev.* **1988**, *A38*, 3098–3100.
(42) Perdew, J. P. *Phys. Rev.* **1986**, *B33*, 8822–8824. Erratum: Perdew, J. P. *Phys. Rev.* **1986**, *B34*, 7406.
(43) Johnson, B. G.; Gill, P. M. W.; Pople, J. A. *J. Chem. Phys.* **1993**, *98*, 5612–5626.
(44) Russo, T. V.; Martin, R. L.; Hay, P. J. *J. Chem. Phys.* **1994**, *101*, 7729–7737.
(45) Grimme, S. *J. Comput. Chem.* **2006**, *27*, 1787–1799.
(46) Ghosh, A.; Gassman, P. G.; Almlöf, J. *J. Am. Chem. Soc.* **1994**, *116*, 1932–1940.
(47) Goff, H. M. In *Iron Porphyrin*; Lever, A. B. P., Gray, H. B., Eds.; Physical Bioinorganic Chemistry Series 1; Addison-Wesley: Reading, MA, 1983; Part I, pp 237−281.
(48) Walker, F. A.; Simonis, U. In *NMR of Paramagnetic Molecules*; Berliner, L. J., Reuben, L., Eds.; Plenum Press: New York, 1993; Vol. 12, pp 133−274.
(49) Bertini, I.; Luchinat, C. In *NMR of Paramagnetic Substances*; Lever, A. B. P., Ed.; Coordination Chemistry Reviews 150; Elsevier: Amsterdam, The Netherlands, 1996; pp 29−75.
(50) Bertini, I.; Luchinat, C. In *NMR of Paramagnetic Molecules in Biological Systems*; Lever, A. B. P., Gray, H. B., Eds.; Physical Bioinorganic Chemistry Series 3; Benjamin Cummings: Upper Saddle River, NJ, 1986; pp 165−229.
(51) Yatsunyk, L. A.; Dawson, A.; Carducci, M. D.; Nichol, G. S.; Walker, F. A. *Inorg. Chem.* **2006**, *45*, 5417–5428.
(52) Nakamura, M.; Tajima, K.; Tada, M.; Ishizu, K.; Nakamura, N. *Inorg. Chim. Acta* **1994**, *224* (1−2), 113–124.
(53) Ikeue, T.; Ohgo, Y.; Ongayi, O.; Vicente, M. G.; Graca, H.; Nakamura, M. *Inorg. Chem.* **2003**, *42*, 5560–5571.
(54) Ongayi, O.; Vicente, M. G. H.; Ghosh, B.; Fronczek, F. R.; Smith, K. M. *Tetrahedron* **2010**, *66*, 63–67.
(55) Ghosh, A. *J. Biol. Inorg. Chem.* **2006**, *11*, 712–724.